

SERVICE BEHAVIOR OF PULTRUDED GFRP MODULAR PANELS APPLIED IN FOOTBRIDGES

Emanuel da Silva Tomás

Department of Civil Engineering, Architecture and Georesources, Instituto Superior Técnico, Technical University of Lisbon, Av. Rovisco Pais, 1049-001 Lisbon – Portugal

October 2011

KEYWORDS

GFRP
Modular panels
Footbridges
Experimental tests
Service behavior
Creep

ABSTRACT

Currently, the construction industry requires quick, economic and durable constructions, along with low maintenance requirements during their service life. In this context, the GFRP modular panels (composite decks) are a good solution in the construction of footbridge decks. This fact relates to the panels' lightness, which makes them easy to handle, as well as their strength and corrosion resistance, which increases their durability and lowers the need for maintenance. Within this work, experimental tests were carried out on small-scale specimens taken from pultruded GFRP modular panels, in order to determine the principal mechanical properties of the laminated material. At the larger scale, GFRP decks, the test programme included flexural (i) static, (ii) dynamic and (iii) creep tests. The aim of the experimental tests was to characterize the service behavior of the slab elements. A failure flexural test was also carried out. Finally, analytical and numerical models were developed and tested, as to describe and predict the behavior of these panels. These models have proved to describe in a satisfactory way the behavior analyzed on the experiments.

1. Introduction

Lightness, low production costs, low maintenance, durability, corrosion resistance and strength are some of the advantages of GFRP (*Glass Fibre Reinforced Polymer*) elements that make them a valid option when choosing solutions for structural projects in general, and bridge decks in particular. The increase of the need of maintenance in traditional bridge decks arose the interest of public entities for alternative technologies. FRP (*Fibre Reinforced Polymer*) decks offer new solutions in this context [1].

Although GFRP and its panels present good properties, as attested by former applications, their utilization is still limited, due to some characteristics of the material that are less advantageous and/or still poorly studied. The susceptibility to instability, the dynamic behavior, the fire behavior (due to the presence of resins) and the creep behavior are some examples such characteristics. It is exactly in the materials' dynamic and creep behavior, but also in its deformability, that lays the focus of the present

dissertation. The investigation carried out in this work aims to contribute to the behavioral description of the deformability, dynamic and creep of pultruded GFRP panels applied in footbridge decks.

The analysis described in this dissertation focus on the pultruded GFRP modular panels (polyester matrix and E-glass) produced by South Korea's *Kookmin Composite Infrastructure* enterprise, under the trade name DELTA DECK™ SF75L, whose main utilization consists of prefabricated footbridge decks.

The primary principle of these panels is based on their particular assembly (figure 1) across the longitudinal direction of the bridge, linking up via an interlock system (snap-fit). The panels should be placed on top of a longitudinal system of reinforced concrete beams, steel or GFRP profiles and its connection is ensured by screwing, which can be enhanced by adhesive bonding.



Figure 1 – Deck assembly by snap-fitting [2].

2. Characterization of the panel's GFRP material

2.1. Panels' geometry

Relatively to their geometry, the panels exhibit a length of 2.50 m (corresponding to the bridge width where they are applied), and a modular transversal section (7 cells) with 90 x 75 [mm] (figure 2). The flange and web walls exhibit a nominal thickness variable between 4 and 5 mm.

Both the main features of the studied panels and the properties related to the geometry of the section are summarized on table 1.

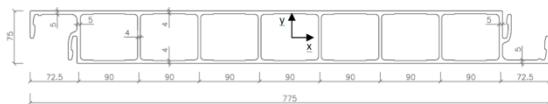


Figure 2 – Transversal section of the slab elements [2].

Table 1 – Geometrical properties of the modular slab elements.

Panel		Section	
L (mm)	2500	A (mm ²)	9661.0
b (mm)	702.5*	A _v (mm ²)	2550.0
h (mm)	75	I _{xx} (mm ⁴)	9151.1 × 10 ³
W (kg)	44.25	I _{yy} (mm ⁴)	1778.5 × 10 ⁶
V (mm ³)	24152.4 × 10 ³	i _{xx} (mm)	30.78
γ _{mat} (kN/m ³)	17.97	W _{xx} (mm ³)	244.03 × 10 ³

* neglecting the width of the tabs due to overlap

2.2. Experimental tests

Even though many properties of a material can be obtained by experimental analysis (physical, chemical, mechanical, durability, fire behavior...), the physical and mechanical properties are the most relevant when trying to characterize the structural strength and the dynamic and creep behaviors of an element containing that material. Thereby, the experimental plan had as primary goals the analysis and characterization of the GFRP material's mechanical and physical properties of the studied pultruded panels.

The other purpose of the experiments was the comparison between the properties of different elements of the panels, such as the flanges and webs, and between its two main directions, the

fibers – *L* and their perpendicular to the laminate plan – *T* (figure 3). In order to fulfill these purposes, specimens were removed from several elements, designated by the following initials: *W* – web; *IF* – inferior flange and *SF* – superior flange. The difference between the superior and inferior flanges is based on their thickness, since the superior flange exhibits an average nominal thickness greater than 4 mm while the inferior flange exhibits an average nominal thickness lower than 4 mm.

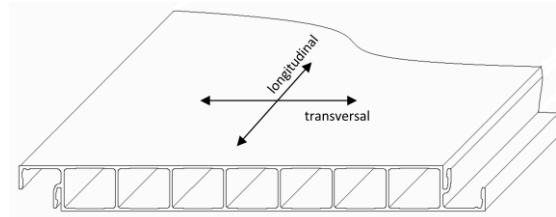


Figure 3 – Panel directions for the removal of the specimens.

The purposes mentioned above were accomplished by carrying out the following tests on each specimen (figures 4 to 9):

- Glass fiber content (Fc specimens);
- Interlaminar shear test (S specimens);
- Bending test (B specimens);
- Tensile test (T specimens);
- Compressive test (C specimens);
- Cell compressive test (Cc specimens).

Standard test methods (applicable to each case) were followed during the execution of these tests [3-8].

The average results of this experimental characterization are presented in table 2, where: σ_u – ultimate stress, σ_{cr} – critical stress; F_{sbs} – laminar shear strength; E - Young's modulus, and the indexes cc – cell compression, f – flexural, t – tensile, L – longitudinal and T – transversal.



Figure 4 – Specimen after calcination.

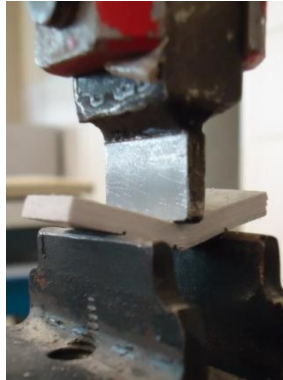


Figure 5 – Interlaminar shear test.



Figure 6 – Bending test.



Figure 7 – Tensile test.



Figure 8 – Compressive test.



Figure 9 – Cell compressive test.

Table 2 –GFRP material's properties.

Fiber content (%)			65.56
Cell compression	Long.	$\sigma_{cr,L}$ (MPa)	110.0
		$\sigma_{ccu,L}$ (MPa)	183.0
Bending	Long.	$\sigma_{fu,L}$ (MPa)	437.6
		$E_{f,L}$ (GPa)	16.6
	Transv.	$\sigma_{fu,T}$ (MPa)	155.4
		$E_{f,T}$ (GPa)	13.2
Tensile	Long.	$\sigma_{tu,L}$ (MPa)	409.1
		$E_{t,L}$ (GPa)	28.8
	Transv.	$\sigma_{tu,T}$ (MPa)	33.6
		$E_{t,T}$ (GPa)	10.1
Laminar shear		F_{sbs} (MPa)	36.4

*The results were inconclusive in the compressive tests.

3. Service and rupture behavior of the panels

As mentioned before, the high deformability and the dynamic and creep behavior are, presently, three features of the GFRP elements that cause great concern and lead to a greater caution in their application as a construction material. Therefore, this chapter is divided in three sections that describe the experimental characterization of the modular panels relatively to those features.

In section 3.1 the short-term static bending behavior of the panels is presented. This characterization involves the determination of

elastic constants and material strengths in order to enable the description of the service and rupture behavior of the panels, particularly maximum resistance, deformation and strain.

In section 3.2 the experimental procedures and results of tests describing the dynamic behavior in bending are reported. The results focus essentially on the determination of the bending and torsion frequencies of the panels.

Finally, in section 3.3 the results for the long term static bending tests (about 1150 h) are presented intended to describe the beginning of the creep phenomenon, are presented. These tests are still in progress.

3.1. Short term bending static tests

3.1.1. Experimental characterization in service conditions

The static tests in panels subjected to bending consisted of the loading of 4 panels (P1-P4), simply supported and loaded at three-point bending configuration, in order to study their service behavior. These tests were conducted based on the European standard method EN 13706 [9] for pultruded profiles.

The load was applied by a Enerpac hydraulic jack (with 200 kN capacity and a maximum stroke of

155 mm). A Novatech load cell, with a capacity of 200 kN, was attached to the hydraulic jack. Three APEK transducers were used to measure displacements (50 mm length and precision of 0.01 mm), and were placed under the transversal alignment of the panel's mid-span (figure 10).



Figure 10 – Instrumentation for the service characterization test.

The registration of loads and displacements was made on a computer using a HBM data acquisition unit with 8 channels, model Spider 8.

Since the studied panels exhibit a length of 2.50 m, the 3 spans were defined as: 1.50 m, 2.00 m and 2.40 m. For each span tested, the load was applied, as displayed in figure 11, until the admissible limit deflection described in the standard document ($L/200$) was achieved, *i.e.*, 7.5 mm, 10.0 mm and 12.0 mm, respectively for the 1.50 m, 2.00 m and 2.40 m spans.



Figure 11 – Test setup for service behavior characterization.

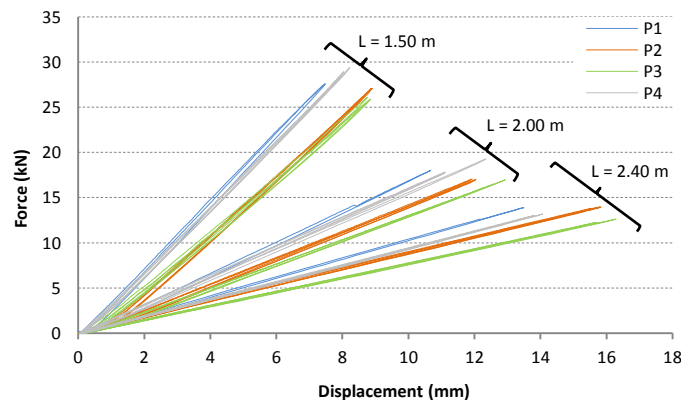


Figure 12 – Force-displacement diagram for the 4 panels.

After the deflection limit was reached, the panel was unloaded, recovering its undeformed state. This cycle was applied 3 times for each span. The force-displacement diagrams (figure 12) represent the results of the load-unload tests applied to these 3 spans. In these diagrams the linear elastic behavior typical of the GFRP elements is perceived.

The effective elastic constants (E_e e G_e) were determined simultaneously, according to the methodology proposed by Bank [10], and also suggested in EN 13706 [9]. The linear regressions of the points determined by this method provide those constants, as shown in figure 13.

As results from the previous methods, the following values are obtained as estimates for the average effective elastic constants:

- $E_e = 30.5 \text{ GPa} \pm 14.0 \%$;
- $G_e = 4.0 \text{ GPa} \pm 30.2 \%$.

Looking at table 3 and its corresponding figure 14, it is verified that, as Bank [10] concluded, the influence of shear deformability decreases with increasing slenderness. The points listed in the table suggest an analogous progress to the curve presented by Bank for an H section with a polyester matrix.

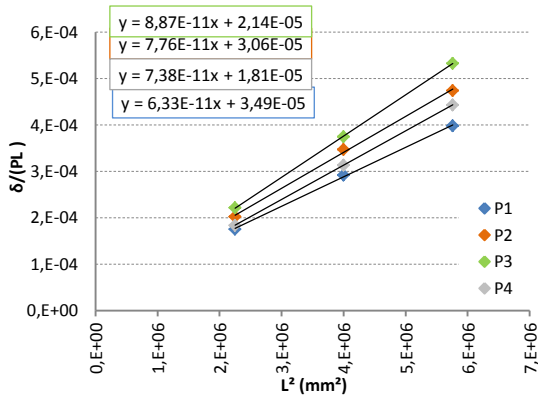


Figure 13 – Diagram to obtain the effective elastic constants.

Table 3 – Shear deformability contribution.

L (mm)	L/i (-)	E _a /E _e (-)	Shear deformability contribution (%)
1500	48.73	0.87	13.0
2000	64.98	0.91	8.8
2400	77.97	0.94	5.6

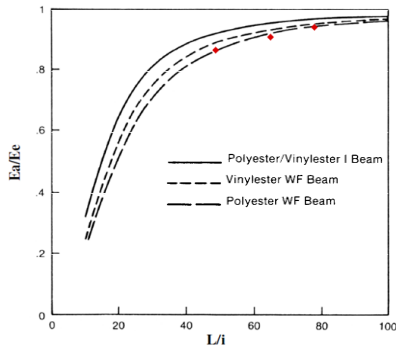


Figure 14 – Influence of shear deformability according to the slenderness (adapted from [46]).

3.1.2. Experimental characterization in failure conditions

In the rupture test the P1 panel was loaded at 4 point bending configuration. In this test, the displacement was only measured at the center of the panel, through an MG transducer, with a maximum measurement capacity of 100 mm. Six TML transducers were also used; in each side of the panel, two strain gauges were placed in the longitudinal direction (at 1/3 and 2/3 of the panels width), and one in the transverse direction. The loading was carried out monotonically in strength control till the rupture of the panel occurred, at an approximate speed of 0.65 kN/s.

The P1 panel revealed a linear behavior up to rupture point, as shown in figure 15. The disruption of the first fibers was audible to a load of about 80 kN, and the collapse of the panel happened for an ultimate load of 118.9 kN and a displacement at mid-span of 29.81 mm ($\approx L/50$). The ultimate main

values that characterize the panel at rupture are summarized on table 4. In this table, the variables are the following: M_u – ultimate moment at mid-span (PL/6); m_u – ultimate moment at mid-span, distributed along the panel’s width; p_u – equivalent ultimate load distributed over the span and along the panel’s width (determined from m_u); σ_u – ultimate tensile stress at mid-span; ϵ_u – ultimate strain in the top surface (SS) and in the bottom surface (IS).

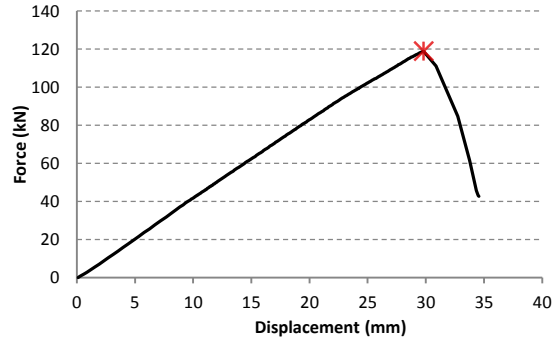


Figure 15 – Force-displacement diagram for the failure test.

Table 4 – Limit values for resistance and deformation.

M_u (kN.m)	m_u (kN.m/m)	p_u (kN/m ²)	σ_u (MPa)	ϵ_u ($\times 10^{-6}$)
29.7	42.3	150.4	121.8	-4135.2 (SS) 3410.3 (IS)

Figure 16 illustrates the rupture of the panel, which occurred near a load application point and corresponds to delamination by local instability of the compressed flange, preceded, presumably, by the crushing of one of the webs (web crippling).

3.2. Dynamic tests

The test was conducted on a 5th panel (P5), simply supported on the spans used in the previous experiment (1.5 m, 2.0 m and 2.4 m). The support system was identical to the one presented above, differing only in the placement of clamps to hold the panel slightly to the sheet metal support. The clamps were used to avoid the bouncing of the panel during percussion.

The accelerometers (Endevco and Bruel & Kjaer) were placed at the intersection between the longitudinal center of each end cell and the mid-span alignment.

The vibration on the panel was induced in two different ways: first by percussion (by a hand blow), and then by releasing of the panel from its deformed position (by suspending a mass of 20 kg and immediately releasing it). In the induction of the percussion, the vibration was

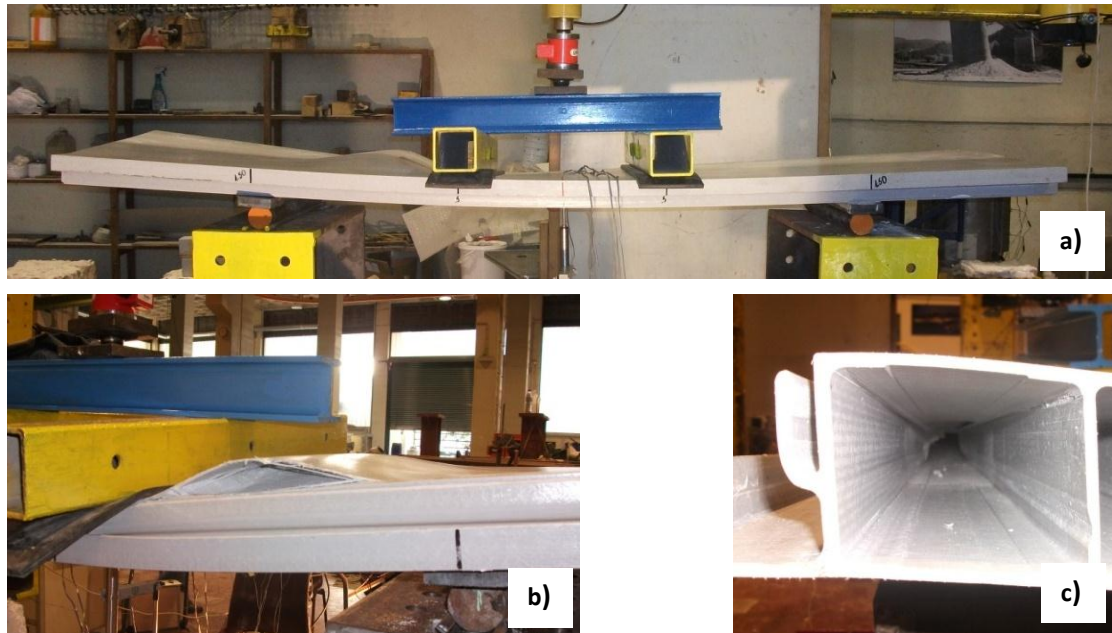


Figure 16 – Panel rupture: a) general view; b) delamination of the compressed flange; c) crushing of a web.

applied in two different points: in the center of the panel, and near one of the accelerometers (eccentric). In the second method (release of deformed position), the vibration was provoked throughout the transversal alignment of the mid-span, using a string that suspended the load, as presented in figure 17. The acceleration was recorded at a frequency of 600 Hz (600 scans per second). For each application point of the vibration, and each span test, the procedure was repeated five times.

Figures 18 and 19 show an example of acceleration *versus* time for the 2.40 m span, with the vibration induced by percussion in the center of the panel, and the corresponding Fast Fourier Transform (FFT) of the average and difference of accelerations, which allowed an estimate of the first bending and torsion frequencies.



Figure 17 – Dynamic test setup.

The analysis of all the FFT's provided the frequencies presented in table 5.

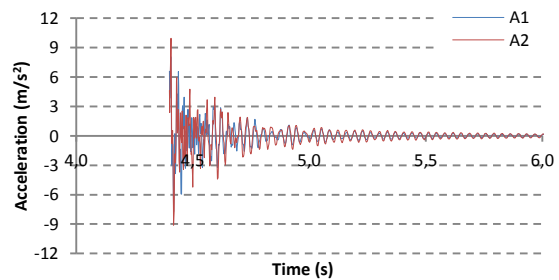


Figure 18 – Panel acceleration in a percussion test at mid-span for the 2.40 m span.

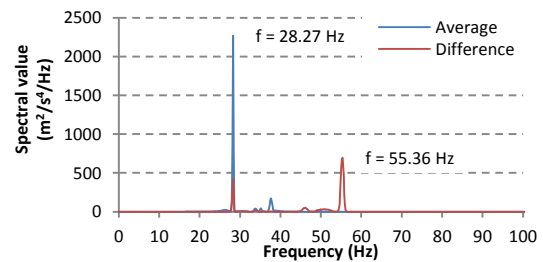


Figure 19 – FFT of the percussion test at mid-span for the 2.40 m span.

Table 5 – Bending and torsion frequencies for each span.

Span	Frequencies (Hz)	
	Bending	Torsion
L = 1.5 m	66.3 ± 0.4 %	111.9 ± 0.4 %
L = 2.0 m	48.2 ± 7.3 %	68.9 ± 6.4 %
L = 2.4 m	31.8 ± 11.9 %	54.7 ± 1.2 %

3.3. Creep tests in panels subjected to bending

The creep tests consisted of reading deformations (longitudinal extensions) and deflections at mid-span of four decks, uniformly loaded with mortar paving slabs (figure 20). The

room environment and GFRP material (of the panels) temperatures were also recorded.

Bituminous sheets (2 mm thick) were placed between the panels and the paving slabs to accommodate small imperfections and minimize the arc effect. Another free load panel was monitored in order to carry out a deformation compensation for the variation of the temperature.

The hinges used in this test were made of two rollers connected by a plate, on top of which the panel was supported, that rolled over an inverted angle iron (figure 21). The fixed supports were materialized by the welding of small metal parts to lock the roller.

The load applied on each element ranged from 500 kgf to 2000 kgf, and is listed in table 6.

The strains were measured with 6 mm TML gauges glued in the center of each panel. The measurements were recorded every 10 s after loading, during the first minute, every 6 min during the subsequent hour, and every hour until it reached 24 hours. From that moment on, the measurements were recorded twice-daily and daily.

The displacements were measured using analog transducers, from the Faku and Mitutoyo brands, with an accuracy of 0,005 mm; the measurements were made manually. The recorded frequencies were identical to those of the extensions, with the exception of the first phase, where the measurements were only recorded every 20 s during the first minute.



Figure 20 – Loading of panels for the creep test.

The results are summarized in table 7, featuring the instant deflections (δ_0) and their increase (%) with time (figure 22).



Figure 21 – Hinges scheme.

Table 6 – Loads applied to each panel.

Panel	L (m)	Load area (m ²)	Load (kN/m ²)	Mass (kg)	% of limit load
CP1	2.0	1.26	5.0	630	3.3 %
CP2	1.5	1.00	10.0	1000	6.6 %
CP3	1.5	1.00	Free	Free	-
CP4	1.5	1.00	20.0	2000	13.2 %
CP5	1.5	1.00	5.0	500	3.3 %

Table 7 – Creep tests displacements.

Panel	CP5 (500 kg)	CP2 (1000 kg)	CP4 (2000 kg)	CP1 (630 kg)
δ_0 (mm)	1.70	2.69	4.94	3.39
24 hours	8.2 %	5.2 %	3.6 %	4.9 %
7 days	10.9 %	7.8 %	5.0 %	7.2 %
90 % of δ_{tot}	9 days	7 days	12 days	22 days

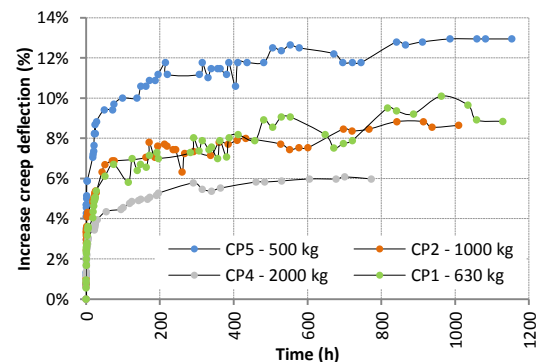


Figure 22 – Creep displacements.

Looking at the diagram presented on figure 22, it can be seen that the panels with higher loads show lower rates of creep displacements. Initially these developments seem a bit different from the expected outcome. However, it is noted that the loading of the panels with the paving slabs was accomplished manually, and thus it was not instantaneous. Therefore, the initial deflection considered here may already include some creep displacement, reducing its growth over time.

In terms of strains, in some cases the results were somewhat unexpected, since there are panels whose records show a decreasing tendency, as shown in figure 23. The results presented in this figure were subjected to a correction, accomplished by the subtraction of the initial records of the free panel's extensions (due to temperature variations).

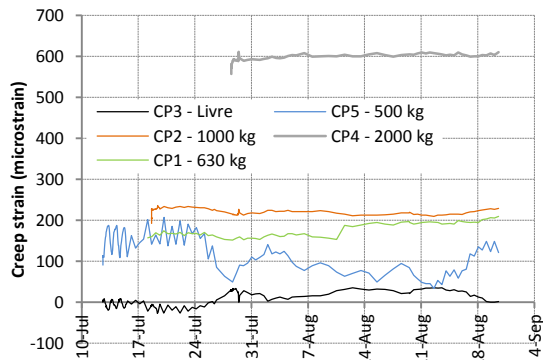


Figure 23 – Creep strain.

4. Numerical and analytical modelling

4.1. Static analysis

The modeling for the study of the deformability was based on analytical and numerical models.

For the analytical model, the Timoshenko beams theory was used. The numerical models were developed in the finite element program SAP2000, version 14.2.4. The numerical models were developed with three-dimensional finite elements, with the GFRP laminate being modeled with thin shell elements.

In the longitudinal direction, the panel flanges were modeled with 20.0 mm finite elements (10.0 mm locally, in the vicinity of loading areas). In the transverse direction, the finite elements representing the flanges exhibit dimensions of 20.0, 25.0 and 35.0 mm, respectively, for the areas of reinforcement in the flange-web connection, flange (normal) and flange in the interlock zone. The finite elements representing the webs exhibit the same dimensions in the longitudinal direction and 30.5 mm in height.

The metal sheets (702.5 x 80 x 25 [mm]) used as support conditions in the experimental phase were simulated as a shell elements (with the steel properties). The mesh used in this case was identical to those used in the flange zone that supports it. The connection between these plates

and the panel was simulated through “joint links”, which only allowed the bending rotation in all the mesh joints.

The GFRP laminate was modeled as an orthotropic material using the values obtained experimentally for its properties, except for those that had not been tested, which were estimated based on bibliography. In order to carry out further analysis to verify the importance of the GFRP properties used in the modeling, three models were developed for each span test. On one of the models the global properties of the material, obtained in tensile tests (GTP), were used. On the other the properties obtained in the same test but differentiating them for each element (web, superior flange and inferior flange) (ETP) were used. On the remaining models the average properties obtained at the panel (PP) in static bending tests were considered. This last model (PP) was developed in order to assess the error associated with lower accuracy in the material properties, since the effective panel properties were used to define the properties of the GFRP laminates.

The application of the models resulted in the values presented in table 8.

Table 8 – Summary of the displacements obtained in the models.

L (m)	Exp. (mm)	Analytical (mm)	ETP (mm)	GTP (mm)	PP (mm)
1.50	7.49	7.10	8.16	7.75	7.48
Δ (%)	-	5.2	8.9	3.5	-0.1
2.00	10.01	9.70	10.85	10.80	10.30
Δ (%)	-	3.1	8.4	7.9	2.9
2.40	12.01	11.98	13.33	13.28	12.63
Δ (%)	-	0.3	10.9	10.5	5.1
1.50*	29.81	31.80	30.76	30.83	29.38
Δ (%)	-	6.7	3.2	3.4	-1.4

*rupture

Figure 24 shows the existing stresses in the panel in the rupture model.

The maximum longitudinal stresses obtained at mid-span are approximately 140 MPa (15% more compared to the experimental tests). A more detailed analysis of the results shows that the area where the rupture occurred is subjected to greater stress (concentration). The webs' compressive stresses and shear stresses obtained by the model (both about 30 to 40 MPa) were somewhat higher than the extrapolated experimental results (22 and 30 MPa, respectively). These differences may be explained

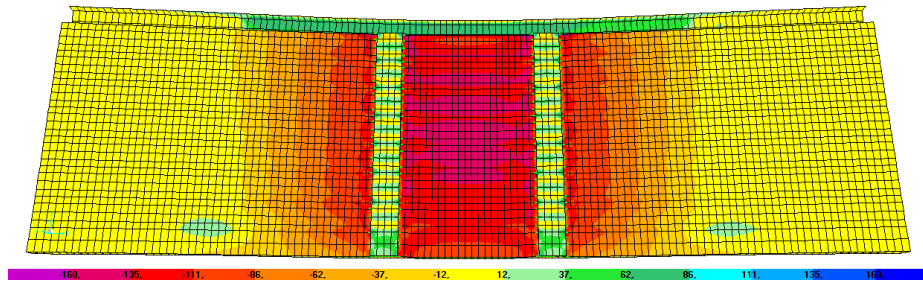


Figure 24 – Longitudinal axial stress in the upper surface in the rupture modelling.

by an eccentricity in the application of the load (in the experimental tests), which lead to a heterogeneous distribution.

4.2. Dynamic analysis

The natural bending frequency of the panel can be obtained analytically, in a simplified form, analyzing it as an oscillator with one degree of freedom. Thus, the frequency can be estimated by the expressions (1) and (2): the first is the general expression for the frequency and the second is a simplified expression for continuous oscillators of simply supported beam elements.

$$f_n = \frac{1}{2\pi} \sqrt{\frac{k}{M}} \tag{1}$$

$$f_n = \frac{2}{\pi} \sqrt{\frac{3 \cdot E \cdot I}{0.49 \cdot \mu \cdot L^4}} \tag{2}$$

In the expression 1, k represents the panel’s bending stiffness (P/δ), which can be obtained by the Timoshenko beams theory, where M is the panel’s mass. In the expression 2, μ represents the mass distributed along the length, L .

The numerical model developed to obtain the dynamic response of the slab elements consisted only of a modal analysis in the numerical program used for each model. The results obtained are presented in table 9.

Examining the results of the table below it can be concluded that the analytical expression (2) provides better estimates of the bending frequencies than the general analytical expression. The differences obtained in comparison with the experimental values may in part be associated with the fact that the damping and the cantilevers effect were neglected, as the models used do not consider them. On the other hand, the models do not consider the shear deformability, which might also affect the deviation observed (that in the

Table 9 –Summary of the frequencies obtained by the models.

		L (m)	1.50	2.00	2.40
Bending frequencies	Experimental		66.3 Hz	48.2 Hz	31.8 Hz
	Analytical model (1)		57.5 Hz	33.3 Hz	23.4 Hz
	Variation		13.3 %	30.7 %	26.6 %
	Analytical model (2)		87.9 Hz	49.5 Hz	34.3 Hz
	Variation		32.6 %	3.0 %	7.9 %
	Numerical Model		67.8 Hz	46.1 Hz	33.0 Hz
Torsion frequencies	Variation		2.3 %	-4.3 %	3.6 %
	Experimental		111.9 Hz	68.9 Hz	54.7 Hz
	Numerical Model		114.8 Hz	79.6 Hz	59.4 Hz
Variation		2.6 %	15.5 %	8.6 %	

expression (2) case is higher for the 1.50 m span, where the influence of this phenomenon is also higher). The numerical models provided accurate results, which means that they are a good solution to estimate the vibration frequencies of the studied panels. The result of these models is less accurate when concerning the torsion frequency of the 2.00 m span with a relative error of 15.5%.

4.3. Creep analysis

The creep modeling was accomplished using the Findley power law [11], expressed in its general and simplified forms by the following expressions, respectively:

$$\varepsilon(t) = \varepsilon'_0 \cdot \sinh\left(\frac{\sigma}{\sigma_\varepsilon}\right) + m' \cdot \sinh\left(\frac{\sigma}{\sigma_m}\right) \cdot t^n \tag{3}$$

$$\varepsilon(t) \approx \sigma \cdot \left[\left(\frac{\varepsilon'_0}{\sigma_\varepsilon}\right) + \left(\frac{m'}{\sigma_m}\right) \cdot t^n \right] \tag{4}$$

where, $\varepsilon(t)$ – total strain in the t instant; ε'_0 – instantaneous strain ε_0 for a reference stress σ_ε ; σ – applied stress; σ_ε – reference stress used to determine ε'_0 ; m' – creep parameter m for a reference stress σ_m ; σ_m – reference stress used to determine m' , and n is a material constant (varies between 0 and 1 for elastic solid and viscous solid behaviors, respectively).

Given the non-expectable results for the strain obtained experimentally, a model based on the extensions estimated by the results of the measured displacements was developed. The power curves in logarithmic scales that best fit the estimated strains, from which m and n parameters were determined, are represented in figure 25.

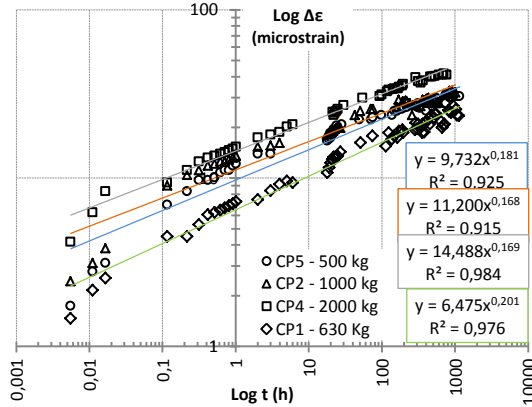


Figure 25 – Panel's m and n parameters' assessment.

Examining the diagram above, the good ability to reproduce the results obtained by the Findley law is verified, also proven by the respective correlation coefficients (R^2). From the analysis of those expressions, which reflect the approach curves, and by applying the simplified Findley model, the average values of instantaneous elastic (E_0) and transient (E_t) moduli were obtained, as well as their ratio (β) and the material coefficient (n) – presented in table 10.

Table 10 – Findley power law creep parameters.

Panel	$n_e = n_d$ (-)	E_0 (GPa)	E_t (GPa)	β (-)
Average	0.18	19.9	751.1	36.5
CV	8.5%	18.6%	40.2%	27.7%

The n parameter obtained is closer to the value obtained by Mottram [12] (0.22) and McClure and Mohammadi [13] (0.17), than those of other authors, whose results point to values higher than 0.30 [14-16].

The elasticity modulus as a function of time can then be estimated by the following expression:

$$E(t) = \frac{E_0 \cdot E_t}{E_t + E_0 \cdot t^{n_e}} \quad (5)$$

The application of the expression to the obtained results marks the decrease in the value of the constant as seen in figure 26.

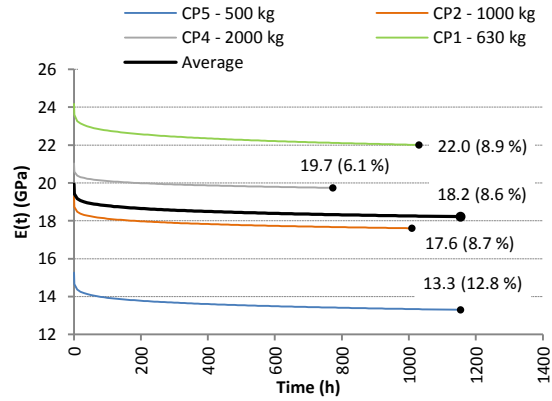


Figure 26 – Elasticity modulus throughout the test period.

In order to assess the importance of simplifying the model, that is, not considering the higher order terms for the first Taylor series, a linearization of the exact model was carried out, from which resulted the curves of figure 27. The almost complete overlap of the models demonstrates that the linearization of the Findley model (that is, the simplification), leads to a good approximation of the results in this particular case.

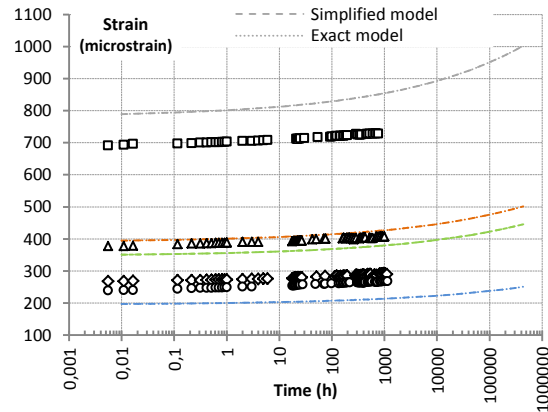


Figure 27 – Findley long term prediction curves.

The reduction factors of the elastic modulus, $\chi(t)$, given by the relation $E(t)/E_0$, were determined. The progress presented by it is showed in figure 28. The average value obtained (0.78) proves to be much higher than the one obtained by Sá *et al.* [16] in their analysis (0.50). However, analyzing the case from a conservative approach, and taking into account the CP5 panel curve of figure 28, it is considered that up to 50 years, a reduction factor of 0.70 should be considered instead.

In order to predict its long term behavior, the Time-Stress Superposition Principle (TSSP) was also applied. Based on accelerated characterization methodology, this principle allows the long term assessment of low stress

level strains with short duration tests (for high stress level applied). The principle is governed by the following expressions:

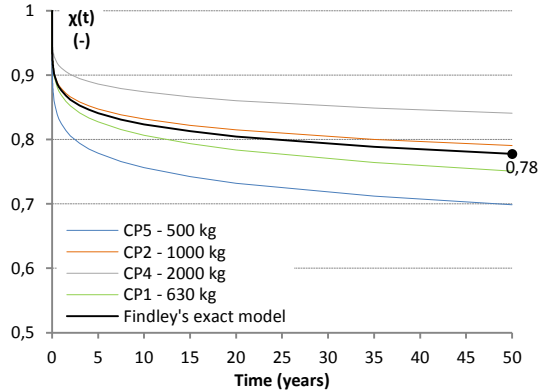


Figure 28 – Long term reduction factors.

$$\varepsilon(\sigma, t) = \frac{1}{a_V} \cdot [\varepsilon_0(\sigma) + m(\sigma) \cdot (t \cdot a_H)^n] \quad (6)$$

$$a_V = \frac{\varepsilon_0(\sigma)}{\varepsilon_0(\sigma_0)} \quad (7)$$

$$a_H = \left(\frac{\varepsilon_0(\sigma_0) \cdot m(\sigma)}{\varepsilon_0(\sigma) \cdot m(\sigma_0)} \right)^{\frac{1}{n}} \quad (8)$$

where, $\varepsilon(\sigma, t)$ – TSSP strain in function of time t , and applied tension σ ; a_V – vertical displacement factor; ε_0 – instantaneous strain due to the applied stress; m – transient strain amplitude due to the applied stress; a_H – horizontal displacement factor; n – Findley law material constant.

The implementation of the TSSP allowed predicting curves for an equivalent loading to that of the CP5 panel for periods longer than 3.5 years (figure 29). The curves are quite consistent with each other and close to the experimental results. Estimating the creep deformation of the PF5 panel for 50 years would require an experimental test of 450 days in a panel with a 1.50 m span and 2000 kg of load (CP4).

Finally, an analysis of the displacements recorded through the adaptation of Euler-Bernoulli equation was made, making it similar to the Findley law:

$$\delta^{E-B}(t) = \left[\frac{5}{384} \cdot \frac{P \cdot L^4}{E_0 \cdot I} \right] + \left[\frac{5}{384} \cdot \frac{P \cdot L^4}{E_t \cdot I} \right] \cdot t^{n_d} \quad (9)$$

The application of the expression (9) and the comparison with the simple prediction of Findley's power law led to the curves of figure 30. The results are very satisfactory for the loading of 630 kg ($L = 2$ m), with differences lower than 20 % in the remaining panels.

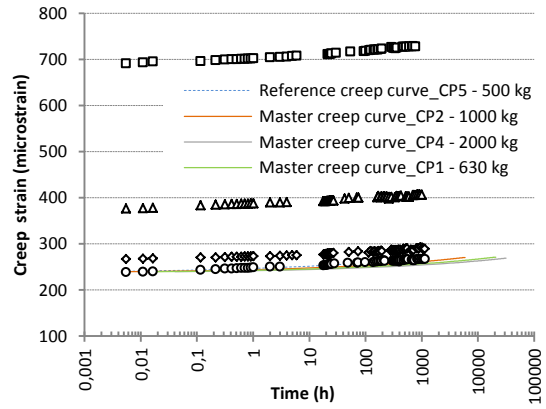


Figure 29 – Prediction curves obtained by the TSSP.

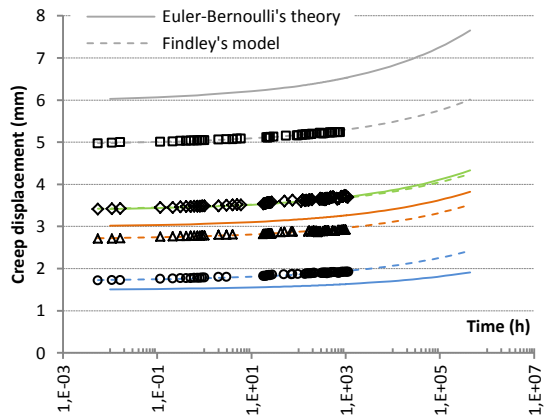


Figure 30 – Creep displacement prediction curves.

5. Conclusions

This study provided an improvement on the understanding of some aspects of the behavior of pultruded GFRP decks. In both experimental characterization of the GFRP material and evaluation of effective elastic constants, the results obtained comply with the ranges previously obtained by other authors.

On the rupture test, the panel's resistance was almost 120 kN, which reveals a high strength of the panels under consideration taking into account their field of application. The dynamic study revealed fundamental frequencies values of 30 Hz, approximately. The creep assessment showed less positive results in the strain records; nevertheless, the deflections evolved as expected. The modeling, in general, presented good approximations compared to experimental results.

References

- [1] Knippers, J., Gabler, M. (2007), "New design concepts for advanced composite bridges - The Friedberg Bridge in Germany", *IABSE Reports*, Vol. 92, 332-333.
- [2] Lee, S.W., Hong, K.J., Kim, J.I. (2008), "Use of the promising composite 'Delta Deck' for various composite-deck bridges",

Fourth International Conference on FRP Composites in Civil Engineering (CICE2008), Zurich.

[3] ISO 1172 (1996), "Textile-glass-reinforced plastics – Prepregs, moulding compounds and laminates – Determination of the textile-glass and mineral filler content – Calcination methods", International Organization for Standardization, Genève.

[4] EN ISO 14130 (1997), "Fibre-reinforced plastic composites: Determination of apparent laminar shear strength by short-beam method", Comité Européen de Normalização (CEN), Brussels.

[5] ISO 14125 (1998), "Fibre-reinforced plastic composites – Determination of flexural properties", International Organization for Standardization, Genève.

[6] ISO 527-1 (1993), "Plastiques – Détermination des propriétés en traction – Partie 1: Principes généraux", International Organization for Standardization, Genève.

[7] ISO 527-4 (1997), "Plastics – Determination of Tensile Properties – Part 4: Test conditions for isotropic and orthotropic fibre-reinforced plastic composites", International Organization for Standardization, Genève.

[8] ASTM D 695-02 (2002), "Standard test method for compressive properties of rigid plastics", American Society for Testing and Materials, West Conshohocken.

[9] CEN - EN 13706-2 (2002), "Reinforced plastics composites – Specifications for pultruded profiles - Part 2: Methods of test and general requirements", European Committee for Standardization, Brussels.

[10] Bank, L.C. (1989), "Flexural and shear moduli of full-section fiber reinforced plastic (FRP) pultruded beams", *Journal of Testing and Evaluation*, Vol. 17, No.1, 40-45.

[11] Findley, W.N. (1960), "Mechanism and mechanics of creep of plastics", *Journal of Polymer Engineering Science*, Vol. 16, No. 1, 57-65.

[12] Mottram, J.T. (1993), "Short- and long-term structural properties of pultruded beam assemblies fabricated using adhesive bonding", *Composite Structures*, Vol. 25, No. 1-4, 387-395.

[13] McClure, G., Mohammadi, Y. (1995), "Compression creep of a pultruded E-glass reinforced plastic angles", *Journal of Materials in Civil Engineering*, Vol. 7, No. 4, 269-276.

[14] Bank, L.C., Mosallam, A.S. (1992), "Creep and failure of a full-size fibre reinforced plastic pultruded frame", *Composites Engineering*, Vol. 2, No. 3, 213-227.

[15] Shao, Y., Shanmugam, J. (2004), "Deflection creep of pultruded composite sheet piling", *Journal of Composites for Construction*, Vol. 8, No. 5, 471-479.

[16] Sá, M.F., Gomes, A.M., Correia, J.R., Silvestre, N.P. (2011), "Creep behavior of pultruded GFRP elements – Part 2: analytical study", *Composite Structures*, Vol. 93, No. 9, 2409-2418.